AFRL-AFOSR-VA-TR-2024-0179

Wall-bounded streamwise vortex destruction

TYLER VAN BUREN
UNIVERSITY OF DELAWARE
220 HULLIHEN HALL
NEWARK, DE, 19716
USA

02/27/2024
Final Technical Report

Air Force Research Laboratory
Air Force Office of Scientific Research
Arlington, Virginia 22203
Air Force Materiel Command

REPORT DOCUMENTATION PAGE

PLEASE DO NOT RETURN YOUR FORM TO THE ABOVE ORGANIZATION.

1. REPORT DATE	2. REPORT TYPE	3. DATES COVERED	
20240227	Final	START DATE 20220930	END DATE 20230929

4. TITLE AND SUBTITLE
Wall-bounded streamwise vortex destruction

5a. CONTRACT NUMBER	5b. GRANT NUMBER	5c. PROGRAM ELEMENT NUMBER
	FA9550-22-1-0438	61102F
5d. PROJECT NUMBER	**5e. TASK NUMBER**	**5f. WORK UNIT NUMBER**

6. AUTHOR(S)
Tyler Van Buren

7. PERFORMING ORGANIZATION NAME(S) AND ADDRESS(ES)
UNIVERSITY OF DELAWARE
220 HULLIHEN HALL
NEWARK, DE 19716
USA

8. PERFORMING ORGANIZATION REPORT NUMBER

9. SPONSORING/MONITORING AGENCY NAME(S) AND ADDRESS(ES)	10. SPONSOR/MONITOR'S ACRONYM(S)	11. SPONSOR/MONITOR'S REPORT NUMBER(S)
Air Force Office of Scientific Research 875 N. Randolph St. Room 3112 Arlington, VA 22203	AFRL/AFOSR RTA1	AFRL-AFOSR-VA-TR-2024-0179

12. DISTRIBUTION/AVAILABILITY STATEMENT
A Distribution Unlimited: PB Public Release

13. SUPPLEMENTARY NOTES

14. ABSTRACT
Wall-bounded streamwise vortex destruction methods were explored using unsteady jets. In application, wall-bounded vortex structures can reduce lift, increase drag, and also decrease stability. In our experiments, we generate longitudinal streamwise vortex structures using tabstyle rectangular vortex generators. Downstream, we use unsteady jets---commonly referred to as synthetic jets---to destroy the incoming vortex structure. Vortex generator interaction with an unsteady jet shows that the synthetic jet can diminish the coherent vorticity of pre-existing vortex structure. We explore a parameter space of rectangular jet orifice pitch and skew angles to inhale coherent vortex structure and exhale weaker vortex structure. Different jet and vortex generator combinations were experimentally explored using particle image velocimetry. All jet orientations were capable of diminishing the incoming coherent vortex structure.

15. SUBJECT TERMS

16. SECURITY CLASSIFICATION OF:			17. LIMITATION OF ABSTRACT	18. NUMBER OF PAGES
a. REPORT U	b. ABSTRACT U	c. THIS PAGE U	UU	13

19a. NAME OF RESPONSIBLE PERSON	19b. PHONE NUMBER *(Include area code)*
GREGG ABATE	

Standard Form 298 (Rev.5/2020)
Prescribed by ANSI Std. Z39.18

Report Coversheet

Award Number

FA9550-22-1-0438

Report Type

Final Research Performance Progress

Reporting Periods

Start 01 October 2022 - End 30 September 2023

Distribution Statement

Distribution A - Approved For Public Release

Program Officer Name

Dr. Gregg L. Abate, AFOSR/RTB

Principal Investigator Name

Dr. Tyler Van Buren, University of Delaware

Project Title

Wall-bounded Streamwise Vortex Destruction

Abstract

Wall-bounded streamwise vortex destruction methods were explored using unsteady jets. In application, wall-bounded vortex structures can reduce lift, increase drag, and also decrease stability. In our experiments, we generate longitudinal streamwise vortex structures using tab-style rectangular vortex generators. Downstream, we use unsteady jets—commonly referred to as synthetic jets—to destroy the incoming vortex structure. Vortex generator interaction with an unsteady jet shows that the synthetic jet can diminish the coherent vorticity of pre-existing vortex structure. We explore a parameter space of rectangular jet orifice pitch and skew angles to inhale coherent vortex structure and exhale weaker vortex structure. Different jet and vortex generator combinations were experimentally explored using particle image velocimetry. All jet orientations were capable of diminishing the incoming coherent vortex structure.

I. Accomplishments

The primary task was to develop a flat plate model, equipped with vortex generators and synthetic jet actuators, with the capability to tune the pressure gradient. Following the physical model fabrication, we conduct measurement data using Stereoscopic Particle Image Velocimetry (SPIV). SPIV provided 3 components of velocity in two-dimensional planes. We explored streamwise data sets to explore the downstream development of the flow field features. Our planned experiments included characterization of the vortex size and shape as it develops downstream for the vortex generator in both a laminar and turbulent environment. Next, we explore the baseline flow fields for the synthetic jet in a laminar or turbulent boundary layer to compare to literature and validate. Then, we collect a data set of the interaction between the vortex generator and the synthetic jet and perform analysis showing vortex destruction in laminar flow with synthetic jet orifice orientation, strength, and location as variables considered. The ideal strength and location of the actuator relative to the vortex for successful destruction is the primary finding. Similar to the previous task, we would also like to explore the interaction of a synthetic jet and vortex generator in a turbulent boundary layer.

We successfully showed a vortex destruction strategy using synthetic jets in a laminar boundary layer. To demonstrate this, we first collected baseline flow fields where we looked at either the vortex generator or the synthetic jet flow field. Vortex generator size and strength was varied using different 3D printed rectangular inserts. We focused most of our studies on a single vortex generator size to conduct more cases for a single incoming vortex. The synthetic jets had varying orifice orientations and blowing ratios. We found that all of our orifice orientations were capable of destroying the pre-existing vortex structure. The orientations had varying degrees of wake penalty, introducing a trade-off of destruction effectiveness against flow slowdown. The downstream development showed that the vortex destruction occurred within ten vortex diameters downstream of the jet orifice.

The results of these studies were recently presented at the American Physical Society, Division of Fluid Dynamics (DFD) 2023 research conference. This is the annual DFD meeting, one of the largest conferences in fluid dynamics. We submitted a technical abstract and performed a 10 minute in-person presentation in Washington, DC. The abstract was titled "Wall-bounded vortex destruction using unsteady actuators on a flat plate" and can be found either on google scholar or through the American Physical Society website for the event. Another conference presentation is planned for the American Institute of Aeronautics and Astronautics (AIAA), SciTech 2024 conference. This conference entails both a 15 minute presentation and a conference paper. We have already submitted the conference paper and are awaiting publication. Going forward, we plan to adapt these results towards a refereed journal article in either AIAA, the Journal of Fluid Mechanics, or Experiments in Fluids. In total, we have two conference presentations and one conference publication with a planned journal publication.

II. Impacts

This work provided insight on a novel flow control technique. While the interactions of vortex generators and jets have been previously studied. None have explored the vortex destruction technique outlined in this study. Previous works have either enhanced the vortex or reversed (relative to our study) which flow control device was upstream. As outlined in the previous section, this work will be a part of two conference presentations and one conference publication, with a journal publication in the works. These works are in the top conferences and journals to maximize impact and reach.

This project provided financial support to hire undergraduate researchers. One of the undergraduate researchers, Alysa Hutton, was a non-binary person of color. They were helpful in developing

the virtual model of the experimental test setup in CAD software. For fabrication, they learned how to design for 3d printing and then how to slice and print their designs. To make larger parts, they assisted in using a CNC router for acrylic and plywood cutting. Finally, they learned how to conduct literature review at a graduate level when performing background research for this study. Another student, Julia Komorowski, was tasked with helping to fabricate a small-scale wind tunnel. They learned how to design accurate assemblies in CAD and then translate them to physical parts through 3D printing and CNC routing. With little training, they were capable of operating independently with high-level tasks outlined. Julia learned about how to design wind tunnels, such as the intricacies of the flow cleaning section, through literature review. Julia is graduating in the Spring of 2024 with her Bachelor's of Science in Civil Engineering and plans to further her studies with a Masters in Mechanical Engineering.

III. Changes

The planned data acquisition technique was Stereoscopic Particle Image Velocimetry. The majority of the data were collected this way. However, a student irreparably broke one of the two cameras. Following this, we switched to planar PIV, losing the in-plane velocity component measurement. The interaction between a single vortex and the synthetic jet was more interesting than initially anticipated. We decided to devote more time to exploring this parameter space in a laminar boundary layer rather than transitioning to turbulent boundary layer experiments.

The proposed facilities experienced unforeseen delays in construction so we were forced to travel to another university to collect data. Data were collected at Hofstra University in their low speed windtunnel. The wind tunnel had a cross-section of 12 in × 12 in with a length of 24 in. This wind tunnel was of a sufficient size to ensure we were far enough away from the closest boundary and also achieved the required freestream velocity range of $5 - 15$ m/s. Because we had to travel to Hofstra University (Hempstead, NY) from the University of Delaware (Newark, DE), we encountered unexpected travel costs.

IV. Technical Updates

A rectangular tab-style vortex generator was investigated. While multiple vortex generators were explored, we present a complete data set for a single vortex generator. We varied the orifice pitch (angle between the orifice wall-normal centerline and the wind tunnel floor) and skew (angle that orients the orifice either along the flow direction or perpendicular to the flow). For all orientations and vortex generator combinations the freestream velocity of the wind tunnel was held constant at $U_\infty = 10$ m/s. The jet blowing ratio $C_b = U_o/U_\infty$, defined as the time-averaged jet output velocity normalised by the freestream velocity, was varied from 1 to 1.3.

A. Methods

Here we investigate the interaction between a tab-style rectangular vortex generator and an unsteady jet along the floor of a wind tunnel. The wind tunnel was an Aerolab EWT open return suction wind tunnel with a turbulence intensity less than 0.25%. The wind tunnel featured a square 30.5 cm × 30.5 cm cross section with a length of 61 cm. A free stream velocity of $U_\infty = 10$ m/s was monitored using a pitot-static tube connected to a Scanivalve DSA3217 multimanometer. The uncertainty of the multimanometer was 2.5×10^{-3} kPa, corresponding to velocity errors of ±0.2 m/s.

The vortex generator had length $l_{\mathrm{VG}} = 40$ mm, width $w_{\mathrm{VG}} = 4$ mm, and height $h_{\mathrm{VG}} = 7.5$

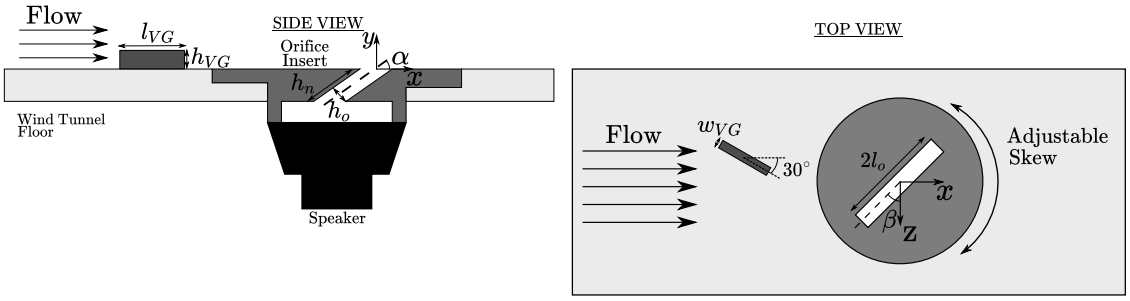

Fig. 1 Schematic showing the wind tunnel floor modifications made to house our test apparatus. Object scales exaggerated for clarity.

mm. The vortex generators were located 210 mm upstream of the orifice center with a spanwise (z-direction) offset of 40 mm. This spanwise offset was chosen by laterally changing the vortex generator location to achieve vortex structure that passed over the center of the synthetic jet orifice. We are considering the role of lateral positioning of the vortex generator. Distances are measured from the centroid of the vortex generator to the center of the orifice slot.The vortex generator was angled at 30° relative to the incoming flow.

Our unsteady jet apparatus consisted of a single Visaton SC 8N speaker attached to an orifice insert plate. The orifice plates had a width of $h_o = 2$ mm, slot length $2l_o = 18$ mm, and neck height $h_n = 7/\sin\alpha$ mm. We tested three separate orifice pitch angles, $\alpha = 45°, 90°$, and 135° by swapping out the orifice inserts. The orifice skew was adjusted by rotating the orifice insert, we explored skew angles $\beta = 0°$ and 30°. The speakers were driven with a sinusoidal voltage signal at a frequency of 220 Hz. The sinusoidal voltage was generated using a Siglent SDG 1032X arbitrary waveform generator and amplified via a Fosi Audio TB10D speaker amplifier. The amplifier RMS voltage was monitored using a Keysight U1242B Multimeter (accuracy of 0.09‰). Three jet velocities were set by maintaining voltages of 5, 10, or 15.3 V_{RMS} across the speaker amplifier output. For the baseline synthetic jet flow fields and the interaction cases, we only used the higher voltage to maximize jet interaction, where lower jet velocities are considered in a following study. This resulted in blowing ratios of $C_b = 1.0$ and $C_b = 1.3$ for the pitched $\alpha = 45°$ and wall-normal $\alpha = 90°$ jets, respectively. For nondimensionalizing length scales and velocity scales we use the orifice width and the freestream velocity, respectively.

A commercial LaVision SPIV system was used to obtain two-dimensional planes of three-component velocity measurements at multiple streamwise locations along the wind tunnel. For time-averaged and phase-locked quiescent jet measurement data, planar PIV was performed instead. The quiescent data planes were perpendicular to the orifice slot length, at the midpoint of the slot. Two Imager SX 4M 4 megapixel, 12-bit CCD cameras with a resolution of 2330×1750 pixels were used to capture the flow. The cameras were mounted onto Scheimpflug lens adapters and equipped with Nikon 105 mm focal length lenses with 532 nm ± 10 nm band-pass filters. Flow was seeded using a Rocket Smoke Machine, producing particles $0.2 - 0.3\mu$m in diameter. A Quantel Evergreen 145 mJ/pulse Nd:YAG dual cavity pulsed laser was used to illuminate the seed particles. The two cameras were positioned on either side of the wind tunnel to achieve angles of 80° between the cameras.

Data were post-processed using LaVision DAVIS software. Velocity vectors were computed from cross-correlation of successive pairs of images. Our ensemble time-averaged data consisted of 500 image pairs taken with time steps of 25 μs. The time between successive image pairs was 5.583 Hz to avoid phase-locking the data acquisition to the unsteady jet actuation frequency. For

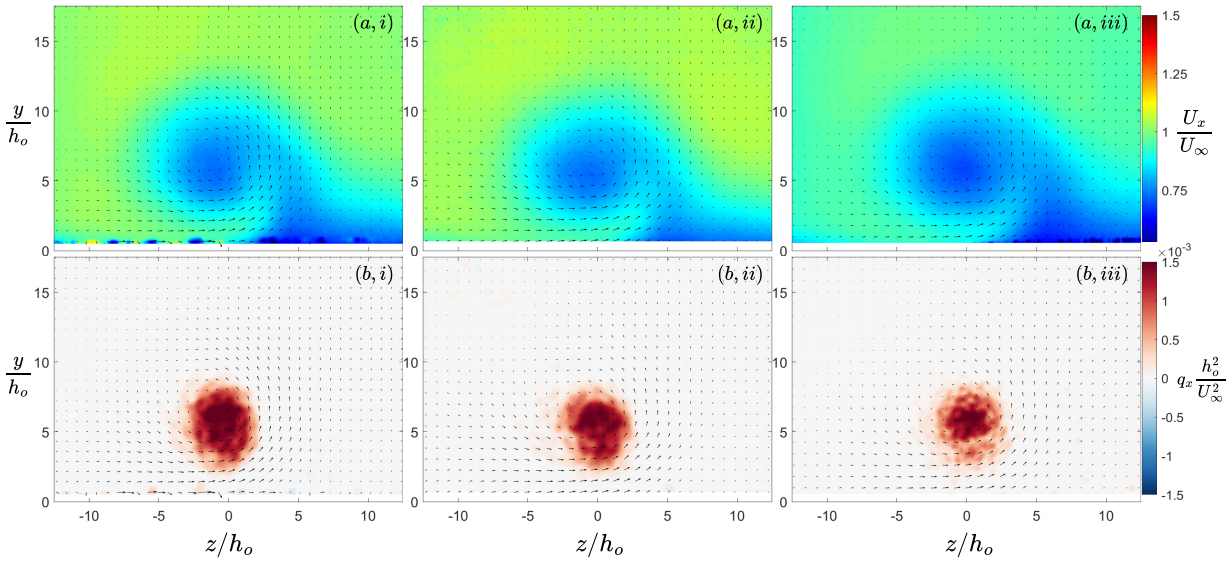

Fig. 2 Contours of normalised streamwise velocity (a) and streamwise vortex structure (b). In-plane velocity vectors are overlaid as black arrows. Downstream development of the vortex generator with height h_{VG} = 7.5 mm. Data were captured at streamwise planes x = 10 mm (i), 20 mm (ii), and 40 mm (iii).

phase-locked data, 500 image pairs were taken with time steps of 5μs. Phase-locked data increments were every 45° from 0 – 315°. A multipass method was used to process the images where the first pass used 48 × 48 pixel interrogation windows with 50% overlap, followed by two passes with 32 × 32 pixel windows with 50% overlap.

B. Discussion

1. Vortex generator characterization

The tab-style vortex generator was used to generate repeatable streamwise vortex structure. The angle of the vortex generator relative to the incoming freestream produced counter-clockwise rotating vortex cores. Our primary focus is on the vortex generator with height h_{VG} = 7.5 mm.

For our qualitative analysis, we typically use two plot styles. To highlight velocity accelerations and deficits, we use contours of the streamwise velocity field normalised by the freestream velocity. When considering vortex structure, we use contours of the streamwise Q-Criterion[1], denoted q_x, colored with the sign of the local vorticity. Both contour figure styles have the in-plane velocity vectors overlaid as black arrows. Starting with the streamwise velocity fields, Figs.2(a,i-iii), the vortex creates a velocity deficit region with a diameter of about twice the height of the vortex generator. The vortex core is rotating counter-clockwise, drawing in and redirecting higher momentum flow from the right. Flow is then accelerated below and to the left of the vortex core, near the floor of the tunnel.

Now we can explore the downstream development of the vortex structure, Figs. 2(b,i-iii). The vortex starts off as a strong core, close to the tunnel floor. The inner diameter, where the vortex is strongest, is on the order of the height of the vortex generator, h_{VG}/h_o = 3.75. As it travels further downstream, the vortex structure weakens and lifts away from the floor. However, the vortex structure is still persistent. Now that we have a general idea of the flow structures produced by just a vortex generator in a crossflow, we can establish the baseline jet flow fields. We will further explore the vortex structure decay when discussing the interaction cases.

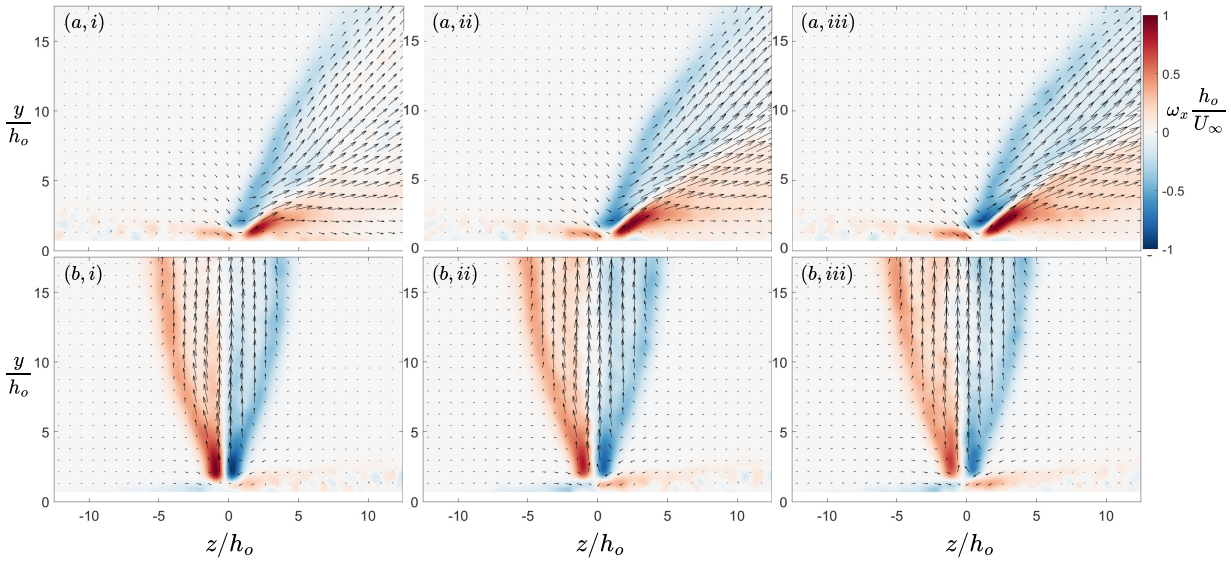

Fig. 3 Vorticity contour field over the synthetic jet orifice perpendicular to the slot length. Black arrows represent in-plane velocity vectors. The different synthetic jet orientations are $\alpha = 45°$ (a) and $\alpha = 90°$ (b). Each column represents a common voltage of 5 V_{RMS} (i), 10 V_{RMS} (ii), or 15.3 V_{RMS} (iii).

C. Synthetic jet characterization

1. Jets in quiescent flow

Quiescent data were taken to better understand the velocity field and vortex production of just the jet. While we focus on four jet orientations when considering interaction cases, here we only need to look at the wall-normal $\alpha = 90°$ and pitched $\alpha = 45°$ orientations—jet skew angles only rotate the resulting velocity and vortex structures in the quiescent field so they would produce the same results. Data planes were perpendicular to the orifice slot length, at the midpoint of the slot. The jet velocity was varied by controlling the power to the speakers. For the time-averaged data near the office, we explored three different power levels, controlled by voltages of 5, 10, and 15.3 V_{RMS}, corresponding to power levels of 3.1, 12.5, and 29.3 W, respectively. The peak voltage was selected to safely operate below the 30 W power limit of the speaker.

First, we can look at contours of streamwise vorticity and in-plane velocity vectors for the 2 orientations and 3 power levels, Fig. 3. Focusing on either the pitched $\alpha = 45°$ or wall-normal $\alpha = 90°$ jet orifice orientations, the resulting velocity fields for all voltages look quite similar. The vorticity appears to be more filled in for the higher voltage cases for either orientation. By that we mean that there is less white space and more either positive (red) or negative (blue) vorticity.

While the differences are hard to discern visually in Fig. 3, we can see a clear trend that jet momentum increases with increased power to the speaker, Fig. 4. (Note that, here we define the jet velocity based upon the crossflow velocity via the blowing ratio, though the jet velocities are calibrated in a quiescent environment.) Both the pitched $\alpha = 45°$ and wall-normal $\alpha = 90°$ orientations have a similar increase in blowing momentum with power. Although, the wall-normal jet initially starts at a higher peak and this offset is present for the three power levels we investigated. Quantitatively, this increase in jet momentum was 92% for the pitched $\alpha = 45°$ jet and 85% for the wall-normal $\alpha = 90°$ jet for an order of magnitude increase in supplied power. While we looked at multiple power inputs to the speaker, we only consider the peak output, corresponding to blowing ratios of 1.0 for the pitched $\alpha = 45°$, 135° or 1.3 for wall-normal $\alpha = 90°$ jets.

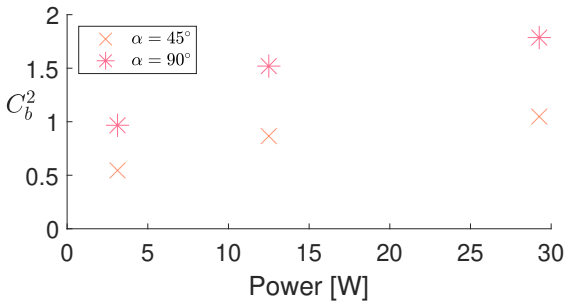

Fig. 4 Variation between jet output momentum, represented here through the blowing ratio squared, and power input for the four orifice inserts.

2. Jets in crossflow

Our qualitative analysis of the synthetic jet baseline flow field focuses on the streamwise velocity field and the streamwise vortex structure. The downstream velocity field, Fig. 5, aligns with previously reported velocity fields for the shared orientations[2].

Starting with the jet pitched along the crossflow direction $\alpha = 45°$, Figs. 5(a,i-iii), we see flow acceleration within the boundary layer. This proposed orientation would likely have the least amount of parasitic effects as this added boundary layer momentum could aid in separation mitigation and control. For the wall-normal jet $\alpha = 90°$ with zero skew $\beta = 0°$, there is a strong wake region just behind the orifice slot at $x = 10$ mm. Flow is accelerated on either side of the jet core, around $z/h_o \approx 4$, Fig. 5(b,i). As the flow evolves downstream this blockage structure lifts away from the wind tunnel floor, causing some flow acceleration below it, at $x = 20$ and 40 mm, Figs. 5(b,ii-iii). For the same pitch angle $\alpha = 90°$ but a different skew $\beta = 30°$, we see similar structures but this time at an angle, Figs. 5(c,i-iii). Finally, an aggressive pitch case of $\alpha = 135°$ and no skew $\beta = 0°$ was considered, Fig. 5(d,i-iii). This jet orientation expectantly produces the largest velocity deficits. Our primary goal with this aggressive pitch orientation was to maximize interaction between the jet and the vortex generator.

The vortex structure produced by the transverse synthetic jets is critical as we would ideally not introduce secondary vortex structures. The downstream vortex structures are shown in Fig. 6. In general, the majority of our orifice orientations produce vortex structures that mostly dissipate by $x/h_o = 40$ mm, with the exception being the wall-normal $\alpha = 90°$ and perpendicular to the crossflow $\beta = 0°$ jet, Figs. 6(b,i-iii). This jet orientation represents a more well studied standard transverse jet case, producing the canonical counter-rotating vortex pair seen for either round or rectangular orifices [3]. For the jet more aligned with the crossflow $\alpha = 45°$, Figs. 6(a,i-iii), we can see weak counter-rotating vortex pairs near the tunnel floor. The skewed wall-normal jet produces strong vortex structure near the orifice, Figs. 6(c,i-iii), but these structures decay more quickly compared to the same pitch jet but perpendicular to the crossflow $\beta = 0°$ orientation. Finally, the jet pitched into the crossflow $\alpha = 135°$, Figs. 6(d,i-iii), has the second weakest vortex structure but a large velocity penalty as noted in previously in Fig. 5.

3. Interaction

With the baseline flow fields established, we can transition to the interaction cases. Our primary metrics will again be the influence on the streamwise velocity field as well as the streamwise vortex structure.

The velocity field downstream of the vortex generator and jet visualizes the wake penalties that

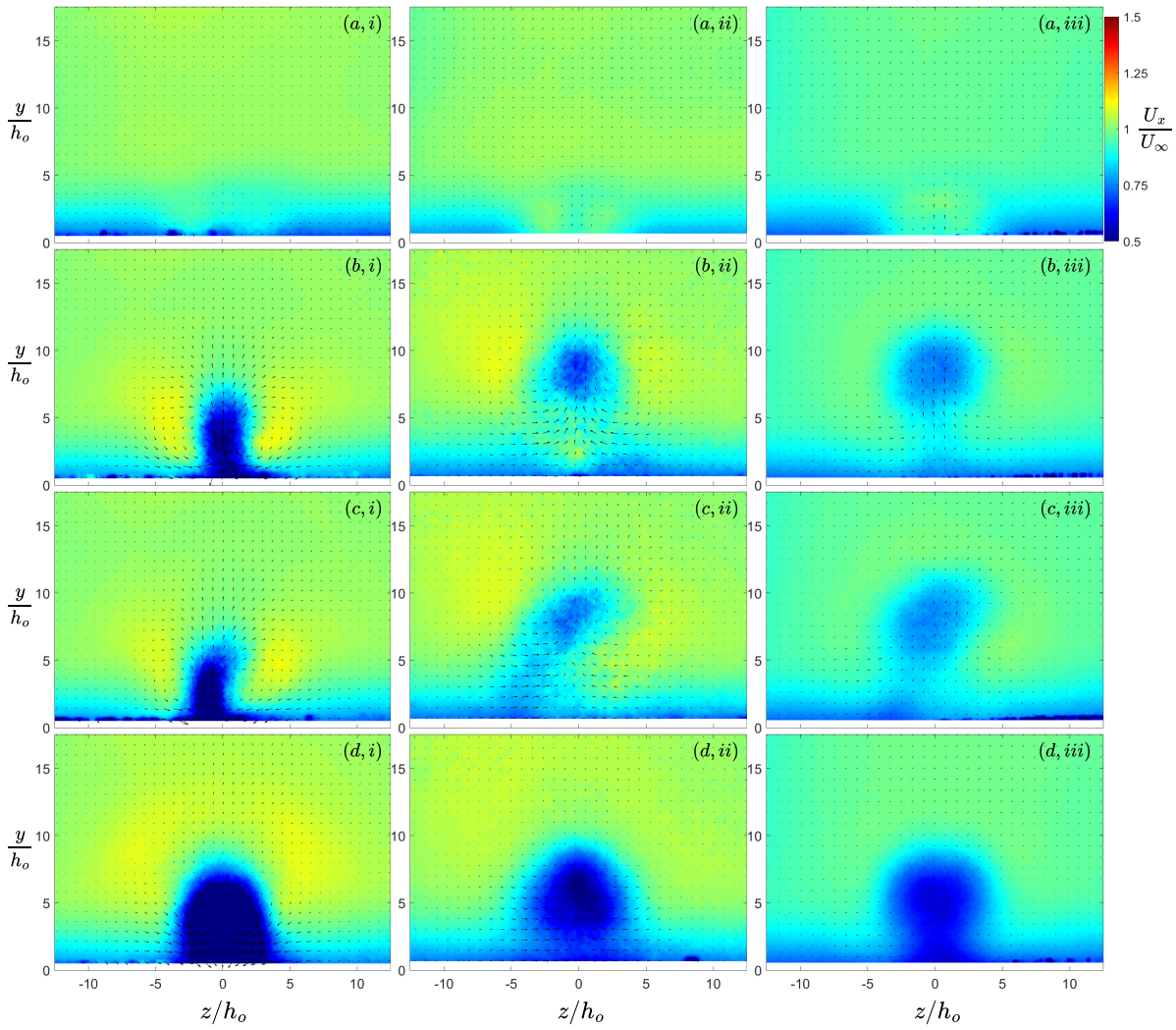

Fig. 5 Downstream development of the velocity field generated by the synthetic jets. The streamwise locations were 10 mm (i), 20 mm (ii), and 40 mm (iii). The different synthetic jet orientations are $\alpha = 45°,\ \beta = 0°$ **(a),** $\alpha = 90°,\ \beta = 0°$ **(b),** $\alpha = 90°,\ \beta = 30°$ **(c), and** $\alpha = 135°,\ \beta = 0°$ **(d).**

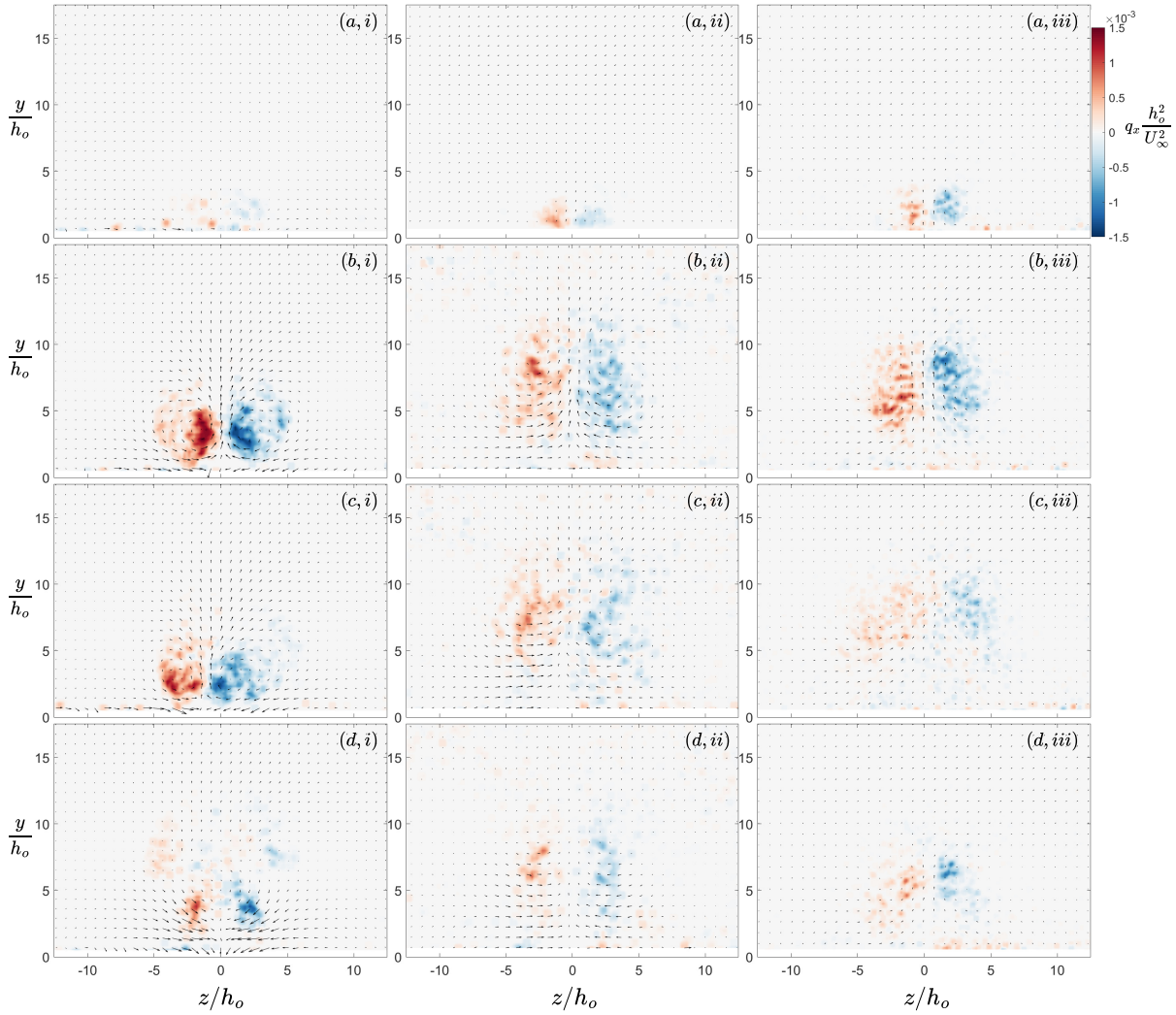

Fig. 6 Downstream development of the vortex structure generated by the synthetic jets. The color contours represent the streamwise Q-Criterion while the overlaid arrows are the in-plane velocity vectors. The streamwise locations were 10 mm (i), 20 mm (ii), and 40 mm (iii). The different synthetic jet orientations are $\alpha = 45°,\ \beta = 0°$ (a), $\alpha = 90°,\ \beta = 0°$ (b), $\alpha = 90°,\ \beta = 30°$ (c), and $\alpha = 135°,\ \beta = 0°$ (d).

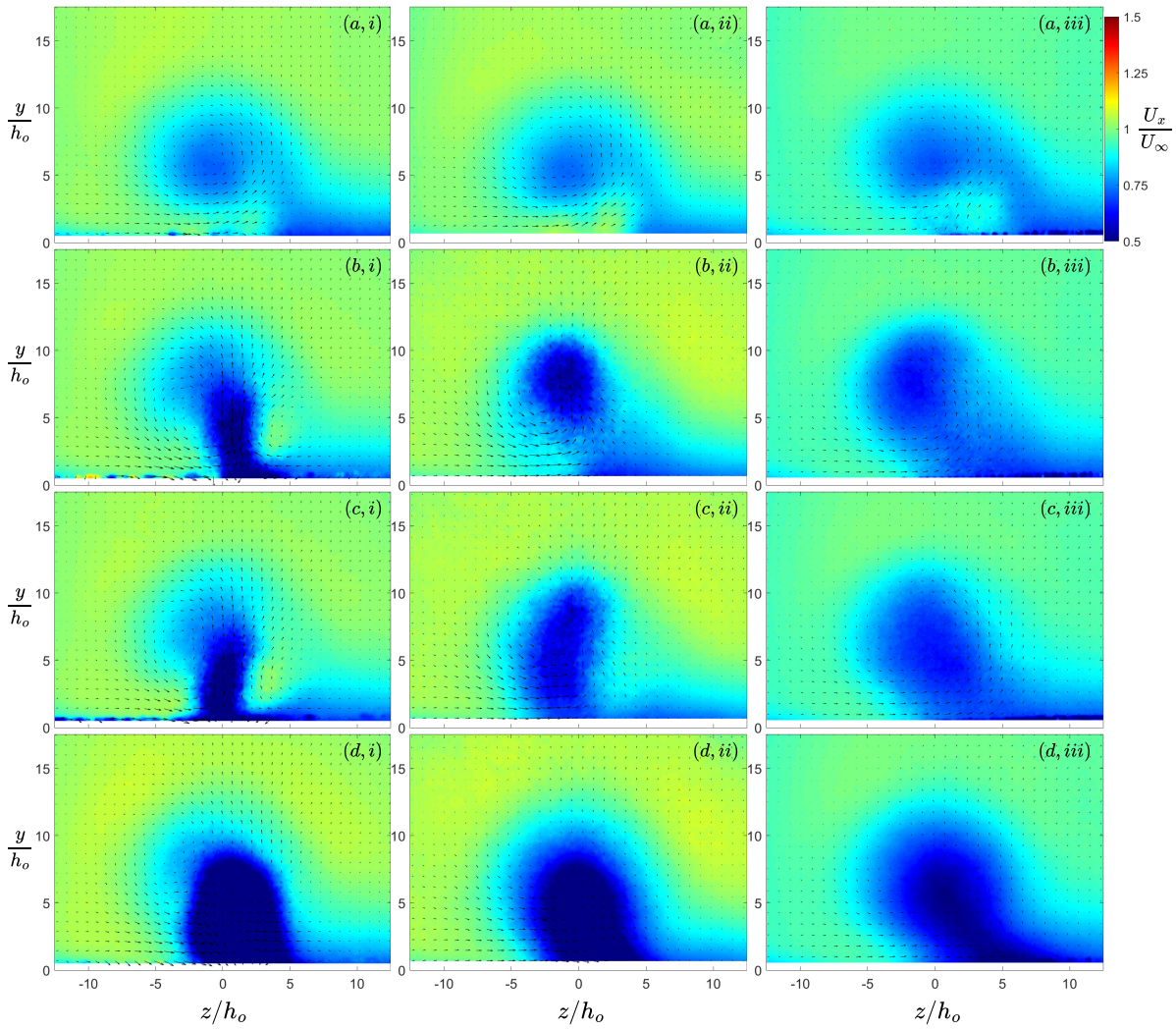

Fig. 7 Downstream development of the velocity field generated through the interaction between the vortex generator and the synthetic jets. The vortex generator had a height h_{VG} = 7.5 mm. The streamwise locations were 10 mm (i), 20 mm (ii), and 40 mm (iii). The different synthetic jet orientations are $\alpha = 45°,\ \beta = 0°$ (a), $\alpha = 90°,\ \beta = 0°$ (b), $\alpha = 90°,\ \beta = 30°$ (c), and $\alpha = 135°,\ \beta = 0°$ (d).

the jets introduce, Fig. 7. All cases show a persistent wake region. However, we do see some wake recovery in the near-wall region for the jet pitched along the crossflow direction $\alpha = 45°$, Figs. 7(a,i-iii). The largest velocity deficit comes from the jet pitched into the crossflow, Figs. 7(d,i-iii), as expected. In general, all wake profiles look similar to the overlaid velocity fields of the baseline cases of just the vortex generator or just the synthetic jet. However, the wake produced by the vortex generator stands out as the more dominant wake for all cases.

Downstream development of the vortex structure, shown through the use of streamwise Q-Criterion, is used to qualitatively gauge vortex destruction, Fig. 8. All jet orientations are capable of breaking up the coherent vortex core into smaller structures. These structures dissipate more rapidly than the original vortex structure as they advect downstream. Major loss of coherence happens within ten vortex diameters. Remnants of the original streamwise vortex are especially visible for the $\alpha = 45°$ jet orientation, Figs. 8(a,i-iii). However, this remaining vortex structure is weaker than the baseline case. The interaction here is entirely favorable as this orientation adds momentum within the boundary layer and generates little additional vortex structure from the interaction between the jet and crossflow. For the wall-normal $\alpha = 90°$ and perpendicular to the crossflow $\beta = 0°$ jet, Figs. 8(b,i-iii), the counter-rotating vortex pair exists in the near field. Further downstream, the vortex structures generated due to the jet dissipate and we are left with a weaker version of the original vortex structure from the vortex generator. The results are even more favorable for the wall-normal $\alpha = 90°$ and skewed $\beta = 30°$ case, Figs. 8(c,i-iii). Throughout the investigated measurement domain, the vortex structure is weaker than the same pitch $\alpha = 90°$ but zero skew $\beta = 0°$ jet orientation. Our most aggressive case, $\alpha = 135°$, fared the best at removing the in-plane vortex structure, Figs. 8(d,i-iii). The biggest drawback for this aggressive pitch orientation is the large velocity deficit it creates, Figs. 7(d,i-iii).

To better compare the downstream streamwise vortex structure, we look at the vortex generator and the four orifice orientations, Fig. 9, at $x = 40$ mm. All cases favorably alter the vortex structure. The aggressive case, Fig.9(c) works quite well at destroying the in-plane velocity components.

D. Conclusion

Coherent streamwise vortex structure was generated using a tab-style rectangular vortex generator in a crossflow. To destroy this pre-existing vortex structure, we used synthetic jets. Data were captured at streamwise locations using stereoscopic particle image velocimetry. For near-field quiescent data, we used planar particle image velocimetry. Jet orientations were selected that would not generate their own coherent vortex structure. The pitched $\alpha = 45°$ or $\alpha = 135°$ jets had a blowing ratio of 1.0 while the wall-normal $\alpha = 90°$ jets had a blowing ratio of 1.3.

The vortex generators produced counter-clockwise streamwise vortex structure that passed over the center of the orifice. Without jet actuation, the baseline flow fields for the vortex generator showed marginal dissipation within our measurement domain. The vortex also generated a large velocity deficit region. Considering synthetic jets alone, most jet orientations produced their own wake regions. The exception was the pitched $\alpha = 45°$ orifice that accelerated flow near the tunnel floor. For most jet orientations, the vortex structure produced was mostly dissipated by $x = 40$ mm. However, the canonical wall-normal $\alpha = 90°$ perpendicular to the crossflow $\beta = 0°$ jet produced counter-rotating vortex pairs that persisted downstream.

Interactions between the vortex generators and the synthetic jets largely grew the wake regions. The jet more aligned with the crossflow $\alpha = 45°$ was the only orientation that initiated wake recovery. The synthetic jets broke up the incoming vortex structure into smaller structures which dissipated more rapidly. All cases favorably reduced the coherent vortex structure. The blowing and suction

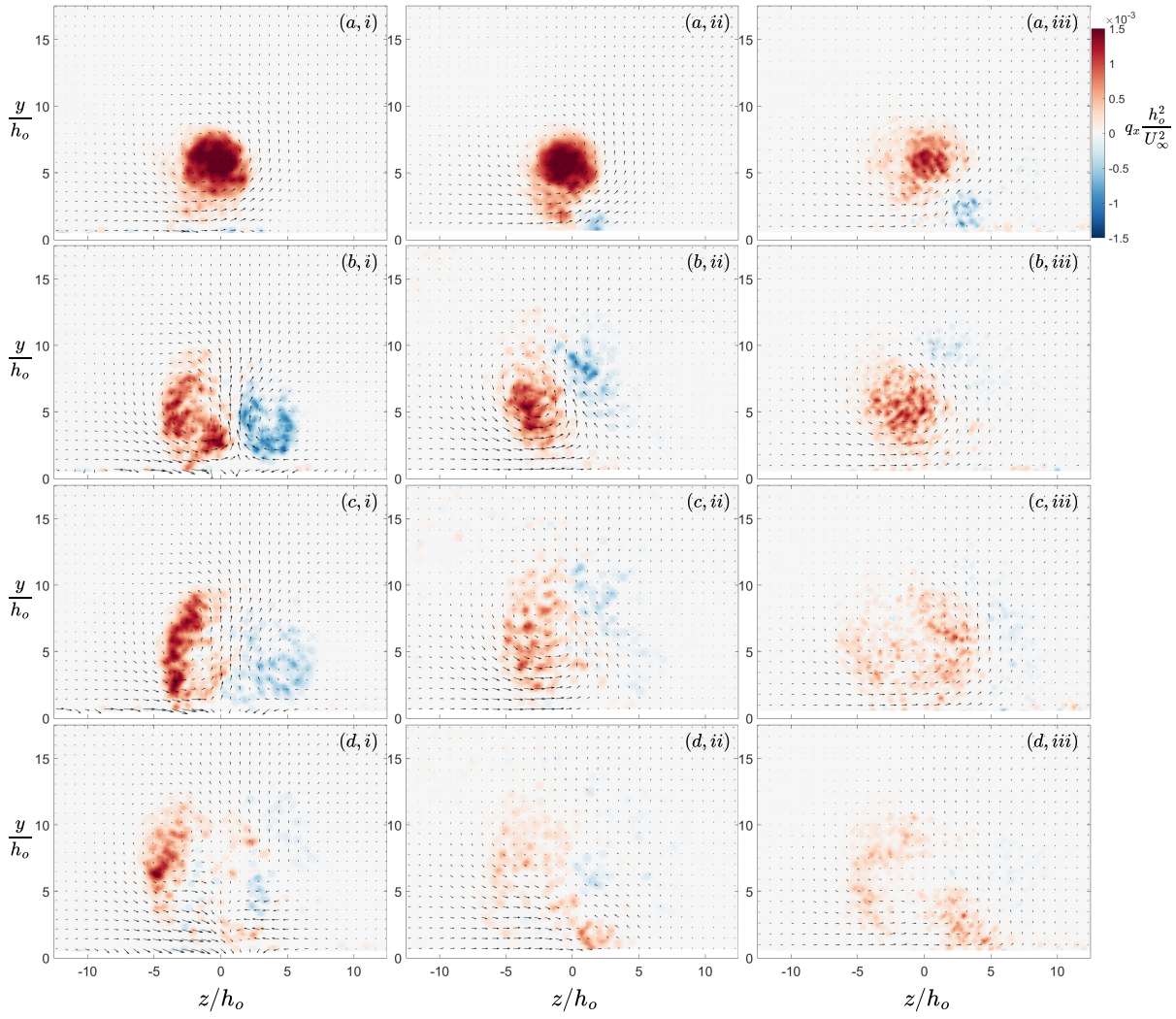

Fig. 8 Downstream development of the vortex structure generated through the interaction between the vortex generator and the synthetic jets. The color contours represent the streamwise Q-Criterion while the overlaid arrows are the in-plane velocity vectors. The vortex generator had a height $h_{\mathrm{VG}} = 7.5$ mm. The streamwise locations were 10 mm (i), 20 mm (ii), and 40 mm (iii). The different synthetic jet orientations are $\alpha = 45°,\ \beta = 0°$ (a), $\alpha = 90°,\ \beta = 0°$ (b), $\alpha = 90°,\ \beta = 30°$ (c), and $\alpha = 135°,\ \beta = 0°$ (d).

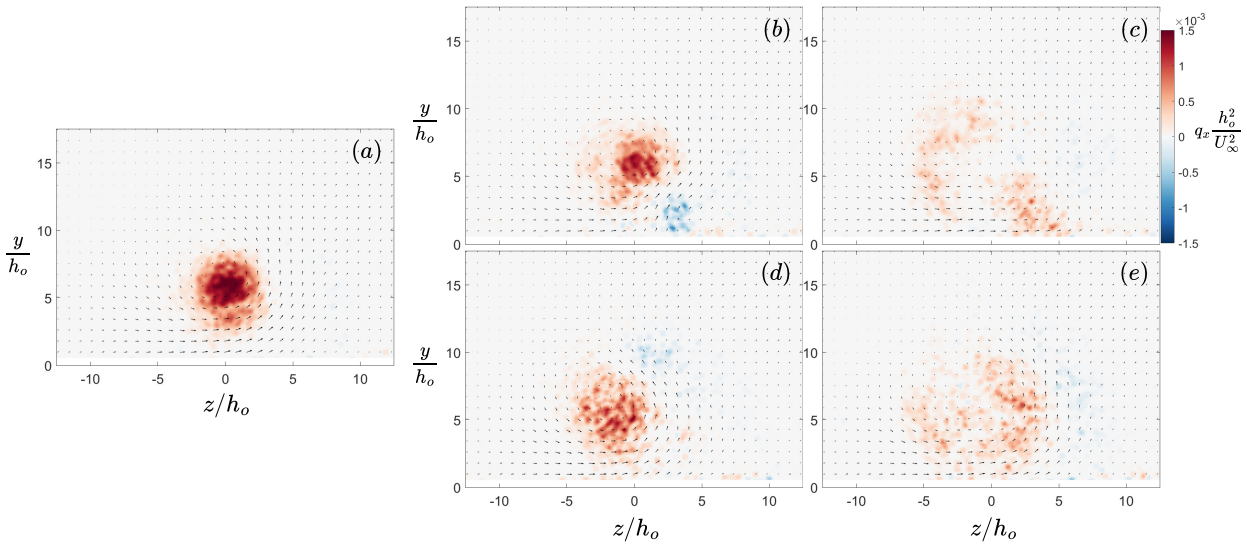

Fig. 9 Far field vortex structure comparison at $x = 40$ mm. Streamwise vortex structure shown for the baseline vortex generator (a), and vortex generator with the following orifice orientations: $\alpha = 45°$, $\beta = 0°$ (b), $\alpha = 135°$, $\beta = 0°$ (c), $\alpha = 90°$, $\beta = 0°$ (d), and $\alpha = 90°$, $\beta = 30°$ (e).

cycles of synthetic jets were leveraged to inhale strong streamwise vortex structure and reorient it as incoherent vortex structure.

Looking to the future, we hope to explore more quantitative aspects of the flow field and directly calculating the pressure recovery of the flow.

Acknowledgments

This work was supported by AFOSR research grant FA9550-22-1-0438.

References

[1] Hunt, J. C., Wray, A. A., and Moin, P., "Eddies, streams, and convergence zones in turbulent flows," *Studying turbulence using numerical simulation databases, 2. Proceedings of the 1988 summer program*, 1988.

[2] Tricouros, F. A., Amitay, M., and Van Buren, T., "Comparing steady and unsteady rectangular jets issuing into a crossflow," *Journal of Fluid Mechanics*, Vol. 942, 2022, p. A56.

[3] Van Buren, T., Beyar, M., Leong, C. M., and Amitay, M., "Three-dimensional interaction of a finite-span synthetic jet in a crossflow," *Physics of Fluids*, Vol. 28, No. 3, 2016, p. 037105.